Journal of Solid State Chemistry 182 (2009) 3031–3040

Contents lists available at ScienceDirect

Journal of Solid State Chemistry

journal homepage: www.elsevier.com/locate/jssc

Structural, magnetic, and thermal characteristics of the phase transitions in $Gd_5Ga_xGe_{4-x}$ magnetocaloric materials

Sumohan Misra [a], Yurij Mozharivskyj [b], Alexandra O. Tsokol [c], Deborah L. Schlagel [c], Thomas A. Lograsso [c], Gordon J. Miller [a,*]

[a] Department of Chemistry and Ames Laboratory, Iowa State University, Ames, IA 50011, USA
[b] Department of Chemistry, McMaster University, Hamilton, ON, Canada L8S 4M1
[c] Ames Laboratory, Iowa State University, Ames, IA 50011, USA

ARTICLE INFO

Article history:
Received 26 May 2009
Received in revised form
4 August 2009
Accepted 8 August 2009
Available online 20 August 2009

Keywords:
Gadolinium–gallium–germanide
Phase transformation

ABSTRACT

Temperature-dependent, single crystal and powder X-ray diffraction studies as well as magnetization, and heat capacity measurements were carried out on two phases of the $Gd_5Ga_xGe_{4-x}$ system: for $x = 0.7$ and 1.0. $Gd_5Ga_{0.7}Ge_{3.3}$ shows three structure types as a function of temperature: (i) from 165 K to room temperature, the orthorhombic Sm_5Ge_4-type structure exists; (ii) below 150 K, it transforms to a orthorhombic Gd_5Si_4-type structure; and (iii) a monoclinic $Gd_5Si_2Ge_2$-type component is observed for the intermediate temperature range of $150\,K \leq T \leq 165\,K$. This is the first time that all these three structure types have been observed for the same composition. For $Gd_5Ga_{1.0}Ge_{3.0}$, the room temperature phase belongs to the orthorhombic Pu_5Rh_4-type structure with interslab contacts between main group atoms of 2.837(4) Å. Upon heating above 523 K, it transforms to a Gd_5Si_4-type structure with this distance decreasing to 2.521(7) Å before decomposing above 573 K.

1. Introduction

Since the discovery of a giant magnetocaloric effect in the pseudobinary $Gd_5(Si_xGe_{1-x})_4$ system [1–8], many intriguing magnetic, crystallographic, and electronic responses have been observed in this family of metal-rich compounds [9–16]. Recent studies reveal that the rich chemistry and physics associated with these compounds are closely related to their two-dimensional structural building blocks and strong magnetoelastic coupling present in these materials [17]. The features that have captured the attention of solid-state chemists are microscopic twinning [18], dependence of crystal structures on the Si/Ge ratio [19,20] and valence electron count [21,22], and their ability to break and re-form covalent bonds existing between pairs of Si/Ge atoms on heating and cooling near the corresponding transition temperatures. This structural behavior has been termed "nanoscale zippers" [23]. The crystal structures of $Gd_5(Si_xGe_{1-x})_4$ and many other RE_5Tt_4 (RE = rare earth; Tt = Si and/or Ge) materials are built from slabs of two eclipsed 3^2434 nets of RE atoms. The arrangements of the atoms in the slabs and, in turn, the structural and magnetic properties depend on the presence or absence of interslab main group–main group chemical bonds.

Three room temperature crystal structures exist for the $Gd_5(Si_xGe_{1-x})_4$ series. The Si-rich compounds ($x \geq 0.56$) adopt the orthorhombic, Gd_5Si_4-type crystal structure [24], and features interslab Si(Ge)–Si(Ge) bonds (distances ca. 2.4–2.6 Å); the Ge-rich compounds ($x \leq 0.3$) adopt the orthorhombic, Sm_5Ge_4-type crystal structure [25] and is characterized by the absence of any interslab Si(Ge)–Si(Ge) bonds (distances exceeds 3.5 Å). The materials in the intermediate composition range ($0.40 \leq x \leq 0.503$) crystallize in the monoclinic $Gd_5Si_2Ge_2$-type crystal structure [26] and has one pair of slabs connected by Si(Ge)–Si(Ge) bonds; however, the other pair do not show interslab Si(Ge)–Si(Ge) bonds. Transformations between different crystal structures can be controlled by changing chemical composition, temperature, magnetic field, and pressure [10,17] and recently, our research group demonstrated the same control by altering the valence electron concentration [21,27].

Electronic structure calculations have suggested the close connection between the structure and magnetic behavior of $Gd_5(Si_xGe_{1-x})_4$ with the number of valence electrons available for metallic bonding [17,28]. Recently, this idea was tested on $Gd_5Ga_xGe_{4-x}$ [21]. It was found that a decrease in valence electron concentration through substitution of three-valent, size-equivalent gallium for four-valent germanium results in reduced population of T1–T1 (Ge–Ge) antibonding states and this leads to steady formation of T1–T1 interslab dimers.[1] This resulted in a

* Corresponding author.
E-mail address: gmiller@iastate.edu (G.J. Miller).

[1] T1–T1 are main group–main group dimers between $^2_\infty[Gd_5T_4]$ slabs. The various structure types observed for the $Gd_5Ga_xGe_{4-x}$ system can be differentiated by the length of these T1–T1 dimer distances.

0022-4596/$ - see front matter © 2009 Elsevier Inc. All rights reserved.
doi:10.1016/j.jssc.2009.08.016

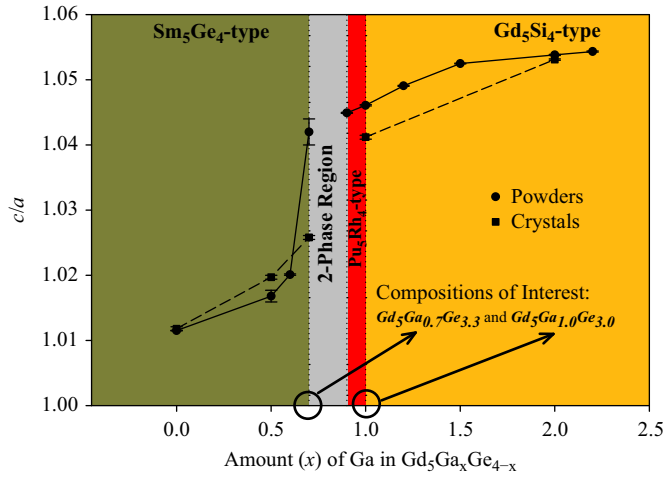

Fig. 1. Variation of c/a with the amount (x) of Ga in $Gd_5Ga_xGe_{4-x}$ at room temperature. The two compositions of interest, $Gd_5Ga_{0.7}Ge_{3.3}$ and $Gd_5Ga_{1.0}Ge_{3.0}$, for the present study are indicated (plot modified from Ref. [21]).

room temperature structural transformation from the Sm_5Ge_4-type ($0 \le x \le 0.9$) to an intermediate, previously unreported, Pu_5Rh_4-type [29] ($0.7 \le x \le 1.0$), and then finally to the Gd_5Si_4-type ($1.2 \le x \le 2.2$), which is indicated by a plot of the lattice constant ratio c/a vs. Ga content x, shown in Fig. 1. Now, to investigate possible effects of temperature on the $Gd_5Ga_xGe_{4-x}$ system, we focused on two compositions, $Gd_5Ga_{0.7}Ge_{3.3}$ and $Gd_5Ga_{1.0}Ge_{3.0}$, which lie, respectively, at the bottom and top ends of the discontinuous part of the c/a vs. x plot (the plotted lattice parameters for $Gd_5Ga_{0.7}Ge_{3.3}$ from powder data belong to Pu_5Rh_4-type and from single crystal data belong to Sm_5Ge_4-type structures. For details see Ref. [21]).

In situ single crystal X-ray diffraction experiments show that $Gd_5Ga_{0.7}Ge_{3.3}$ transforms to a Gd_5Si_4-type structure for temperatures below 150 K. Between 150 and 165 K the monoclinic $Gd_5Si_2Ge_2$-type is also observed. On the other hand, *in situ* powder and single crystal X-ray diffraction experiments show that $Gd_5Ga_{1.0}Ge_{3.0}$ adopts a Pu_5Rh_4-type structure at room temperature and transforms to a Gd_5Si_4-type structure above ca. 523 K. In addition to structural details, we also report results of magnetization and heat capacity measurements for these two compositions.

2. Experimental section

2.1. Syntheses

All weighings were done in air and were then taken inside a glove-box (conc. of $H_2O = 60$–80 ppm) equipped with an arc-melter. All samples studied here were not subjected to any kind of extended heat treatments. Samples were prepared by arc-melting stoichiometric mixtures of high purity constituent elements on a water-cooled copper hearth in an argon atmosphere. The starting materials, pieces of gadolinium (99.99 wt%, Materials Preparation Center, Ames Laboratory [30]) gallium (99.99 wt%, Aldrich), and germanium (99.9999 wt%, Alfa Aesar), were used as obtained. Each ingot had a total weight between 1–3 g and was remelted six times to ensure homogeneity. Weight losses during melting were less than 0.1 wt%. Single crystals of $Gd_5Ga_{1.0}Ge_{3.0}$ were extracted only from the as-cast samples; for $Gd_5Ga_{0.7}Ge_{3.3}$, single crystalline samples suitable for anisotropic physical property measurements were prepared by the Bridgman technique.

To obtain these single crystals of $Gd_5Ga_{0.7}Ge_{3.3}$, a 74 g sample with loaded composition "$Gd_5Ga_{1.0}Ge_{3.0}$" was prepared according to the procedure above with the subsequent alloy drop cast into a copper chill cast mold. Then, the as-cast ingot was electron beam welded in a tungsten Bridgman style crucible [31], and heated in a tungsten mesh resistance furnace under a pressure of 8.8×10^{-5} Pa up to 1973 K. The sample was held at this temperature for 30 min to degas the crucible and charge, after which the chamber was backfilled to a pressure of 3.4×10^4 Pa with high purity argon. The ingot was then heated to 2173 K followed by withdrawal from the heat zone at a rate of 8 mm/hr. Due to separation of Ga and Ge during Bridgman growth, the top part of the ingot was Ga-rich and the bottom part of the ingot was Ge-rich (discussed in detail in later sections). $Gd_5Ga_{0.7}Ge_{3.3}$ single crystals were extracted from both the as-cast ingot and the bottom part of the as-solidified ingot grown by the Bridgman method.

2.2. Powder X-ray diffraction

The as-cast samples were examined by powder X-ray diffraction for identification and to assess phase purity. These initial powder patterns were obtained using an Enraf-Nonius Guinier camera using monochromatized Cu$K\alpha$ radiation ($\lambda = 1.540598$ Å) at 298 K and Si powder (NIST; $a = 5.430940 \pm 0.000035$ Å) as a calibration standard. The purity and homogeneity of all phases were confirmed by comparison of powder X-ray diffraction patterns to those calculated from single-crystal data using the *POWDER CELL* software [32]. Powder patterns at high temperature were collected on a Rigaku TTRAX rotating anode diffractometer using Mo$K\alpha$ radiation ($\lambda = 0.71075$ Å) and equipped with a sample heater in an evacuated chamber. Fine $Gd_5Ga_{1.0}Ge_{3.0}$ powder with particle sizes less than 38 μm was obtained by grinding the ingot in an agate mortar and pestle and then passing through a stainless steel sieve. The resulting powder was mounted on a copper sample holder and the sample was smoothed using a stainless steel razor blade. The scattered intensity was measured as a function of Bragg angle with a scintillation detector, in a step scan mode for 2θ ranging from 9.00° to 42.00° and a stepsize of 0.01° with the intensity measured for 2 s at each point. The sample temperature remained stable within ±1 K with respect to the value set for an experiment. All diffraction patterns collected at various temperatures were analyzed by a full-profile Rietveld refinement using *LHPM RIETICA* software [33]. The scale factor and the lattice parameters of each phase were refined. The coordinates of individual atoms were refined if the amount of the corresponding phase was at least 20 mol%. The isotropic displacement parameters of all atoms in each phase were assumed to be the same. The profile residuals, R_p were from 10.74 to 12.72, and the derived Bragg residuals, R_B were from 6.29 to 7.43.

2.3. Single-crystal X-ray crystallography

Variable-temperature diffraction experiments were performed on $Gd_5Ga_{0.7}Ge_{3.3}$ and $Gd_5Ga_{1.0}Ge_{3.0}$. Several single crystals were extracted from $Gd_5Ga_{0.7}Ge_{3.3}$ (samples grown by Bridgman method and as-cast samples) and $Gd_5Ga_{1.0}Ge_{3.0}$ (as-cast samples) products. To prevent contamination of the crystals at high temperatures, neither glue nor cement was used to mount the crystals; instead, a special procedure was used (Fig. 2), the details of which have been described elsewhere [34]. Room- and high-temperature X-ray diffraction data were collected on a Bruker Smart Apex CCD diffractometer with Mo$K\alpha$ radiation ($\lambda = 0.71075$ Å) and a detector-to-crystal distance of 5.990 cm equipped with a Nonius crystal heater. Low-temperature data were collected on a similar instrument equipped with an Oxford Cryosystems cooler. During the high- and low-temperature diffraction experiments, the temperature remained stable within

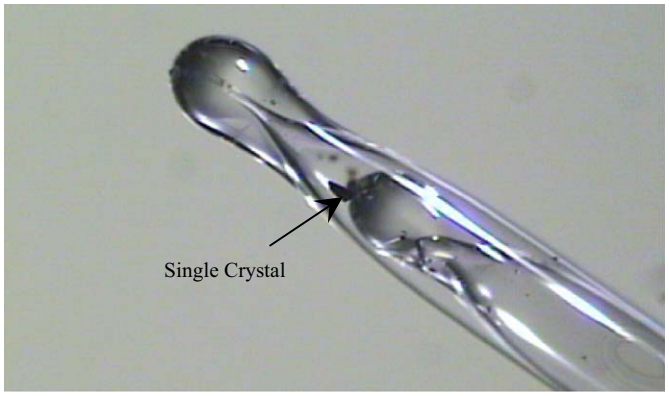

Fig. 2. A picture of a single crystal of $Gd_5Ga_{1.0}Ge_{3.0}$ prepared for high-temperature X-ray diffraction experiments.

± 1 K with respect to the value set for an experiment. Single crystal diffraction data at 143, 293, 298, and 533 K were collected for a maximum 2θ value of 57° either over a full sphere or a hemisphere of reciprocal space, with 0.3° scans in ω and an exposure time of 10 s per frame. Also collected were three sets of 30 frames with similar specifications to obtain the corresponding lattice parameters for various high- and low-temperature diffraction experiments on $Gd_5Ga_{0.7}Ge_{3.3}$ and $Gd_5Ga_{1.0}Ge_{3.0}$, respectively (see supporting information). The *SMART* [35] software was used for data acquisition. Intensities were extracted and then corrected for Lorentz and polarization effects by the *SAINT* [35] program. Empirical absorption corrections were accomplished with *SADABS* [35], which is based on modeling a transmission surface by spherical harmonics employing equivalent reflections with $I > 3\sigma(I)$. Structure solutions and refinements were performed with the *SHELXTL* [35] package of crystallographic programs. Because Ga and Ge atoms could not be unequivocally distinguished by X-ray diffraction techniques in these systems due to the one-electron difference in their electron densities; statistical mixtures of Ga and Ge atoms consistent with sample stoichiometry were assumed on all main group sites during the refinement procedures.

2.4. Magnetic property measurements

Magnetic measurements on single and polycrystalline samples were carried out using a **S**uperconducting **QU**antum **I**nterference **D**evice (SQUID) magnetometer MPMS-XL, manufactured by Quantum Design, Inc. The measurements included dc magnetic susceptibility measurements between ca. 4 and 300 K and isothermal magnetization measurements in dc magnetic fields varying from 0 to 50 kOe. For the susceptibility measurements, the samples were first cooled under zero magnetic field (zfc) and then the measurements were carried out on heating under a 20 or 10 kOe magnetic field. Susceptibility measurements were then repeated upon cooling with the magnetic field turned on (fc).

2.5. Heat capacity measurements

The heat capacities for both $Gd_5Ga_{0.7}Ge_{3.3}$ and $Gd_5Ga_{1.0}Ge_{3.0}$ were measured using a semi-adiabatic heat-pulse calorimeter [36] between ca. 5 and 400 K in dc magnetic fields ranging from 0 to 10 T. Rectangular blocks weighing 0.3833 and 1.2615 g, respectively, for $Gd_5Ga_{0.7}Ge_{3.3}$ and $Gd_5Ga_{1.0}Ge_{3.0}$ were used for the above measurements. For $Gd_5Ga_{0.7}Ge_{3.3}$, oriented single crystals along its [001], [010], and [100] axes were used, whereas for $Gd_5Ga_{1.0}Ge_{3.0}$, as-cast polycrystalline samples were used.

Table 1
Crystallographic data for $Gd_5Ga_{0.7}Ge_{3.3}$ as obtained by single crystal X-ray diffraction (space group *Pnma* (no. 62), Mo*K*α radiation, 2θ range = 4–57°, $Z = 4$).[a]

Temperature (K)	293	143
Structure type	Sm_5Ge_4	Gd_5Si_4
a (Å)	7.6359(5)	7.525(2)
b (Å)	14.855(1)	14.829(4)
c (Å)	7.8079(5)	7.840(2)
V (Å^3)	885.7(1)	874.8(4)
No. of independent reflections	1117	798
No. of parameters	46	46
Final R indices	$R1 = 0.0247$,	$R1 = 0.0685$,
$[I > 2\sigma(I)]$	w$R2 = 0.0557$	w$R2 = 0.1406$
Peak/hole (e/Å^3)	1.714/−1.695	3.704/−6.445
b/a	1.94542(9)	1.9706(4)
c/a	1.02252(9)	1.0419(4)
T1–T1 (Å)	3.405(2)	2.687(7)

[a] Further details of the crystal structure investigation(s) can be obtained from the Fachinformationszentrum Karlsruhe, 76344 Eggenstein-Leopoldshafen, Germany, (fax: +49 7247 808 666; e-mail: crysdata@fiz.karlsruhe.de) on quoting the depository number CSD-420879 and 420880.

Table 2
Atomic coordinates and isotropic displacement parameters for $Gd_5Ga_{0.7}Ge_{3.3}$ as obtained by single crystal X-ray diffraction at 293 and 143 K.

Atom		x	y	z	U_{eq} (Å^2)[a]
293 K					
Gd1	8*d*	0.0106(1)	0.5976(1)	0.1804(1)	0.013(1)
Gd2	8*d*	0.3619(1)	0.1188(1)	0.1642(1)	0.013(1)
Gd3	4*c*	0.1962(1)	1/4	0.5023(1)	0.012(1)
T1	8*d*	0.2038(1)	0.0426(1)	0.4642(1)	0.016(1)
T2	4*c*	0.0668(2)	1/4	0.1111(2)	0.014(1)
T3	4*c*	0.3119(2)	1/4	0.8662(2)	0.013(1)
143 K					
Gd1	8*d*	0.0194(2)	0.5954(1)	0.1819(1)	0.004(1)
Gd2	8*d*	0.3228(2)	0.1226(1)	0.1753(1)	0.003(1)
Gd3	4*c*	0.1530(3)	1/4	0.5106(2)	0.003(1)
T1	8*d*	0.1568(5)	0.0403(2)	0.4696(3)	0.003(1)
T2	4*c*	0.0249(7)	1/4	0.1041(4)	0.003(1)
T3	4*c*	0.2735(7)	1/4	0.8689(4)	0.003(1)

[a] U(eq) is defined as one third of the trace of the orthogonalized U_{ij} tensor.

3. Results and discussion

3.1. Phase transformations in $Gd_5Ga_{0.7}Ge_{3.3}$

Detailed descriptions of the orthorhombic Sm_5Ge_4-type, monoclinic $Gd_5Si_2Ge_2$-type, and orthorhombic Gd_5Si_4-type structures can be found elsewhere [21,23,25,26,29]. Lattice parameters and atomic coordinates for $Gd_5Ga_{0.7}Ge_{3.3}$ at 293 and 143 K, are listed in Tables 1 and 2. Room temperature crystal structure of $Gd_5Ga_{0.7}Ge_{3.3}$ belongs to the Sm_5Ge_4-type with a T1–T1 distance of 3.405(2) Å and $c/a = 1.02252(9)$ (see Table 1), which places it near the bottom of the discontinuous part of the c/a vs. x plot (see Fig. 1) for $Gd_5Ga_xGe_{4-x}$.

Further exchange of Ga for Ge lowers the valence electron count, which formally removes electrons from T1–T1 antibonding states, thus decreasing the T1–T1 dimer distance, resulting in the intermediate Pu_5Rh_4-type structure and eventually, at $x \geq 1.2$, the Gd_5Si_4-type crystal structure [21]. Now, for the fixed composition, $Gd_5Ga_{0.7}Ge_{3.3}$, a related effect was observed by lowering the temperature. The result, as shown in Fig. 3, is a transformation, first to the monoclinic $Gd_5Si_2Ge_2$-type structure for the temperature

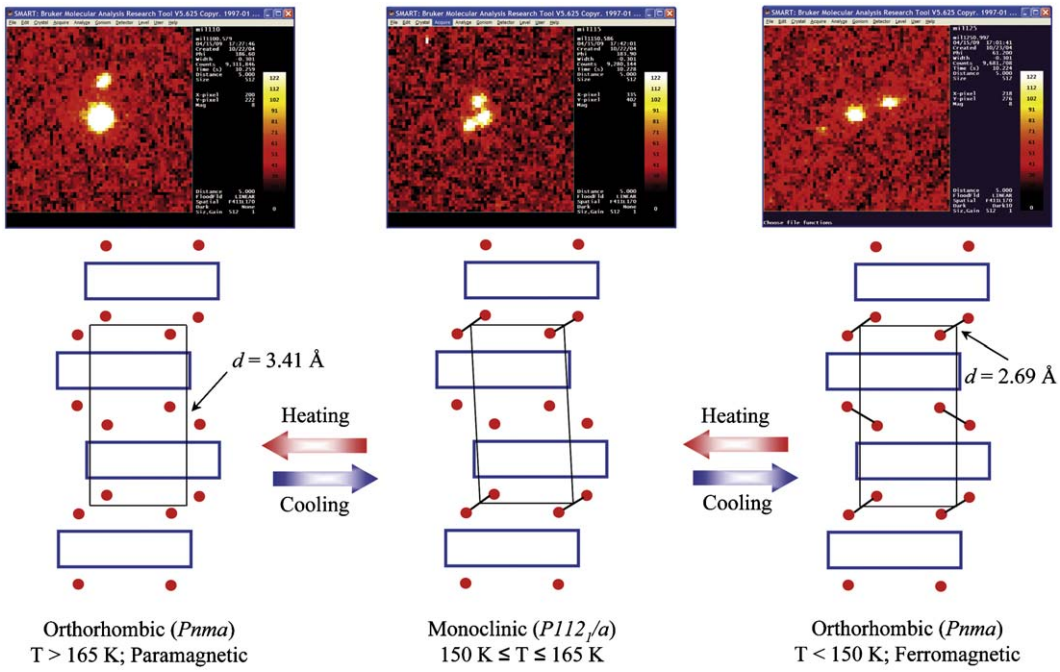

Fig. 3. Schematic representation of the phase transformation in $Gd_5Ga_{0.7}Ge_{3.3}$ as the sample is cooled. The Gd1 and Gd2 network in each slab is shown as the blue "lattice". The CCD diffraction frames show the corresponding reflections of orthorhombic and monoclinic components which were eight times magnified. (For interpretation of the references to color in this figure legend, the reader is referred to the web version of this article.)

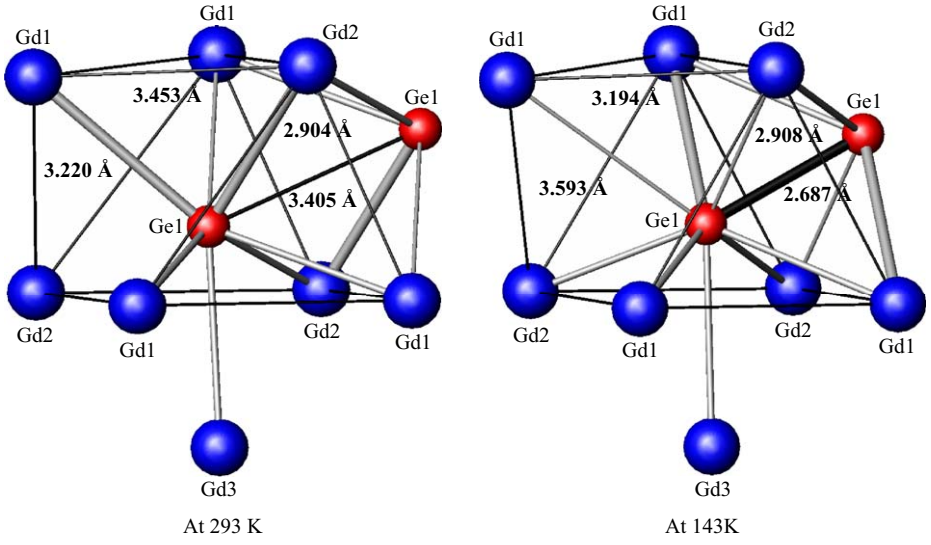

Fig. 4. Coordination environments surrounding the T1 sites for $Gd_5Ga_{0.7}Ge_{3.3}$ as it changes with temperature. Interatomic distances showing significant differences between the structures are included.

range $165\,K \geq T \geq 150\,K$, and then to the orthorhombic Gd_5Si_4-type structure for temperatures below 150 K, where there are short T1–T1 dimers, e.g. a distance of 2.687(8) Å measured at 143 K.[2]

Seven crystal structures, in total, have been reported for RE_5T_4 (RE = rare-earth; T = Ga, Si, Ge, Sn, Sb) materials for various temperatures. They are (i) orthorhombic Sm_5Ge_4-type, (ii) monoclinic $Gd_5Si_2Ge_2$-type, (iii) orthorhombic Gd_5Si_4-type, (iv) tetragonal Zr_5Si_4-type, (v) hexagonal Ti_5Ga_4-type, (vi) orthorhombic Eu_5As_4-type, and (vii) orthorhombic Pu_5Rh_4-type [4,21]. An eighth crystal structure, adopting the monoclinic $U_2Mo_3Si_4$-type [37], also exists for mixtures of rare-earth elements [38,39]. Materials undergo transitions between different crystal structures by changing chemical composition, temperature, magnetic field, pressure, and valence electron count. But, as of yet, we have seen only a maximum of two crystal structure types being stabilized for a particular chemical composition, when the other parameters vary. To our knowledge, $Gd_5Ga_{0.7}Ge_{3.3}$ is the first example for which three structures exist by varying temperature: the orthorhombic Sm_5Ge_4-type, monoclinic $Gd_5Si_2Ge_2$-type, and

[2] During data collection at low temperatures, ice developed over the crystal and due to this, the absorption correction was poor. Also, the total number of independent reflections collected as a result of icing was only 798 and, therefore, the completeness to θ_{max} is 72%. However the R1 and data/parameter values are quite acceptable. Nevertheless, we do observe similar structural transformations for as-cast single crystal samples. The c/a parameters (ca. 1.04) at 143 K for both Bridgman grown and as-cast single crystals lie in the regime of the Gd_5Si_4-type structure as per the structure map in Ref. [19].

orthorhombic Gd_5Si_4-type for the same composition. This exemplifies the degree of flexibility that the $Gd_5Ga_xGe_{4-x}$ system possesses and its ability to stabilize various types of crystal structures.

In the 150–165 K range, $Gd_5Ga_{0.7}Ge_{3.3}$ exhibits the presence of two phases. Near 165 K the monoclinic $Gd_5Si_2Ge_2$-type phase coexists with the Sm_5Ge_4-type structure, while near 150 K, it coexists with the Gd_5Si_4-type structure. Appearance of two diffraction spots around a "central" one was indicative of the development of the monoclinic $Gd_5Si_2Ge_2$-type phase (e.g. coexistence of the orthorhombic and monoclinic modifications of $Gd_5Si_2Ge_2$ at 573 K [34]). The unit cell parameters could be obtained for both the orthorhombic phase associated with the "central" spots and the monoclinic phase associated with the "peripheral" spots (as shown in Fig. 3). Additionally, the orthorhombic and monoclinic phases can coexist as separate crystalline domains within a "single crystal," as we observed in $Gd_5Si_{1.5}Ge_{2.5}$ [23]. However, since the monoclinic phase is typically twinned by single crystal diffraction [17], the presence of an additional orthorhombic component (either Sm_5Ge_4-type or Gd_5Si_4-type) has hampered our ability to refine the monoclinic structure thoroughly.

The coordination environments surrounding the T1 sites above and below the phase transition, illustrated in Fig. 4, are similar to those observed in $Gd_5(Si_xGe_{1-x})_4$ materials [20]. In both structures the T1 site is surrounded by a tricapped trigonal prism of eight Gd atoms and one T1 atom. In the Sm_5Ge_4-type structure at 293 K, with long T1–T1 contacts (ca. 3.405(2) Å), the T1–Gd1 contact capping the trigonal prism is short (ca. 3.220(1) Å). In the Gd_5Si_4-type structure at 143 K, the corresponding T1–Gd1 contact increases to 3.593(1) Å while the T1–T1 distance decreases to 2.687(8) Å. The figure also highlights one of the T1–Gd1 distances within the trigonal prism which decreases from ca. 3.453(1) to 3.194(3) Å. Also, as we have seen with some $Gd_5(Si_xGe_{1-x})_4$ materials [20], the low-temperature structure has a higher symmetry (*Pnma*) than the high-temperature structure ($P112_1/a$). This is in violation of the Gibbs free energy/entropy relationship, which would imply a reverse structural sequence [34], and it may be due to large magnetic exchange energy and subsequent magnetic ordering for the orthorhombic phase, which overcomes the unfavorable entropy contribution [17,28].

To check any possible structural implications at high temperature, we also performed single crystal X-ray diffraction on $Gd_5Ga_{0.7}Ge_{3.3}$ from 298 to 533 K (see supporting information). These experiments do not reveal any structural transition up to 523 K; and, then, at 533 K the crystal no longer gives diffraction intensity.

3.2. Magnetism and heat capacity for $Gd_5Ga_{0.7}Ge_{3.3}$

Magnetic measurements were carried out on single crystalline samples extracted from the bottom part of an ingot grown by the Bridgman method. Fig. 5a shows the temperature dependency of the dc magnetization measured in a magnetic field of 20 kOe in the temperature range of ca. 5–320 K. The plot portrays two interesting features: (1) a dip in magnetization (shown by the arrow) at ca. 160 K, which probably corresponds to the structural phase transition from Gd_5Si_4-type through $Gd_5Si_2Ge_2$-type to Sm_5Ge_4-type; and (2) a change in slope (shown by another arrow) at ca. 195 K, which corresponds to the phase transition between paramagnetic and ferromagnetic states of the high temperature Gd_5Si_4-type phase.

Fig. 5b portrays the temperature variation of the MCE, calculated in terms of the isothermal magnetic entropy change ($-\Delta S_M$) for various field changes (ΔH). The magnetic entropy change was calculated from the $M(H)$ data collected at various temperatures by employing Maxwell's relation as described in Ref. [37]. MCE for $Gd_5Ga_{0.7}Ge_{3.3}$ shows a maximum at ca. 170 K

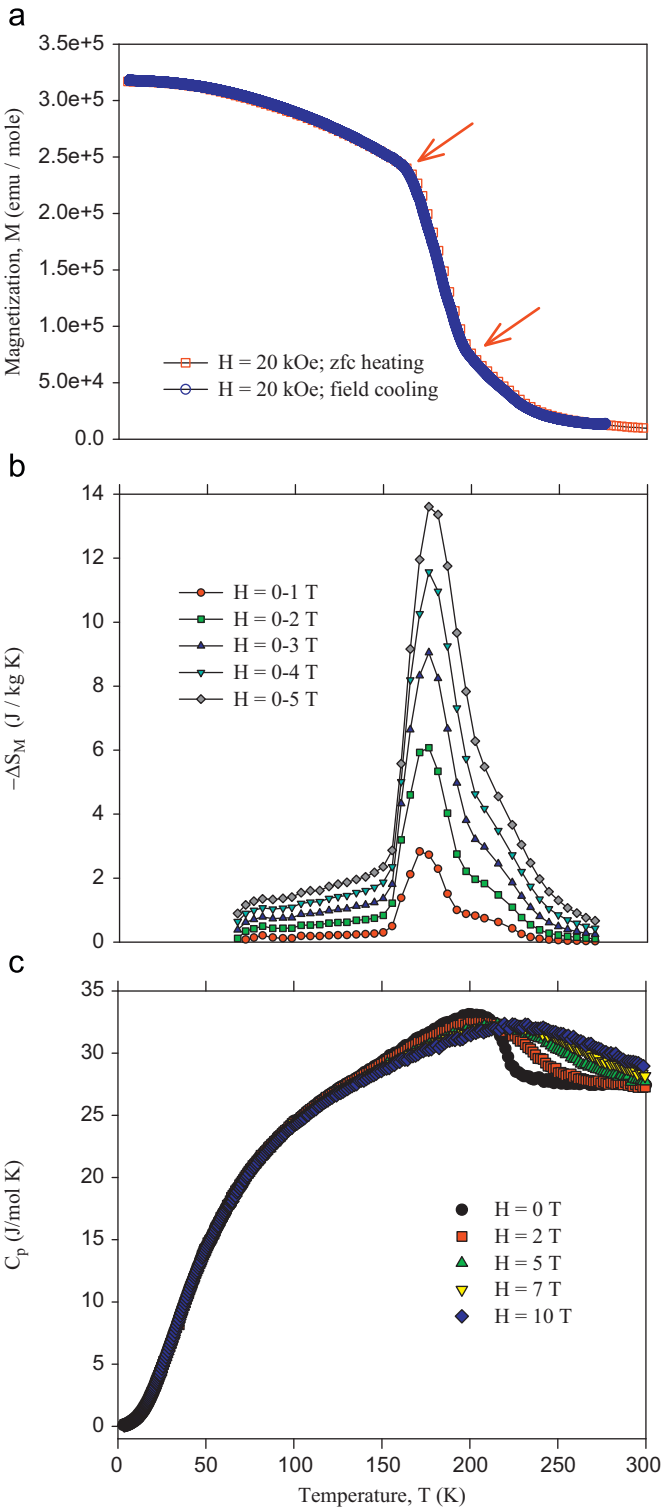

Fig. 5. (a) The magnetization of zero-magnetic-field cooled samples of $Gd_5Ga_{0.7}Ge_{3.3}$ measured as a function of temperature in a stable dc magnetic field of 20 kOe. (b) The magnetic entropy change ($-\Delta S_M$) of single crystalline $Gd_5Ga_{0.7}Ge_{3.3}$ as a function of temperature calculated from magnetic measurements for 1, 2, 3, 4, and 5 T magnetic field changes. (c) The heat capacity of a single crystalline sample of $Gd_5Ga_{0.7}Ge_{3.3}$ oriented along its (001) axis as a function of temperature in 0, 2, 5, 7, and 10 T magnetic fields.

with a peak value of 14 J/kg K. In comparison, $-\Delta S_M$ for $Gd_5Si_2Ge_2$ shows a peak value of 20 J/kg K for $\Delta H = 0$–5 T at 277 K [7].

To further understand the magnetic properties of this compound, we also measured the temperature variation of the heat capacity (C_p), shown in Fig. 5c. The $C_p(T)$ data show a nonλ-type anomaly peaking at ca. 200 K. The peak width is ca. 50 K and reveals that the phase transitions (both structural and magnetic) occur over a wide range of temperature. Both the behavior and location of this anomaly are commensurate with the magnetic measurements shown above.

One of the problems that we encountered during the preparation of this material is an ability to control stoichiometry, specifically, the Ga/Ge ratio. Since $Gd_5Ga_{0.7}Ge_{3.3}$ lies near the boundary of a two-phase region (Fig. 1), preparation of this material typically produces a second Pu_5Rh_4-type phase, suggesting that this compound does not melt congruently. The concentration of this second phase is much smaller in samples prepared by the Bridgman method compared to the as-cast samples. This is probably due to elemental separation of Ga and Ge during Bridgman growth, in which the top part of the ingot becomes Ga-rich and the bottom part becomes Ge-rich [31]. We speculate that this phenomenon inhibits the growth of the second Pu_5Rh_4-type phase in the bottom part of the ingot from which the sample was extracted for the present study, as this second phase only shows up when the Ga content is between 0.7 and 1 for $Gd_5Ga_xGe_{4-x}$. The crystallographic results are similar for both as-cast and samples grown by the Bridgman method, but the magnetic properties, especially $-\Delta S_M(T)$, depreciate significantly for the as-cast samples. Hence, only the results for samples grown by the Bridgman method are presented here.

Table 3
Crystallographic data for $Gd_5Ga_{1.0}Ge_{3.0}$ as obtained by single crystal X-ray diffraction (space group *Pnma* (no. 62), Mo$K\alpha$ radiation, 2θ range = 4–57°, $Z = 4$).[a]

Temperature (K)	298	533
Structure type	Pu_5Rh_4	Gd_5Si_4
a (Å)	7.562(4)	7.672(2)
b (Å)	14.929(7)	15.210(5)
c (Å)	7.904(4)	7.834(2)
V (Å^3)	892.3(7)	914.2(5)
No. of independent reflections	1095	1142
No. of parameters	47	47
Final R indices	$R1 = 0.0527$,	$R1 = 0.0711$,
[$I > 2\sigma(I)$]	w$R2 = 0.0990$	w$R2 = 0.1169$
Peak/hole (e/Å^3)	2.896/−2.859	4.011/−2.795
b/a	1.9742(7)	1.9825(4)
c/a	1.0452(7)	1.0211(4)
T1–T1 (Å)	2.837(4)	2.521(7)

[a] Further details of the crystal structure investigation(s) can be obtained from the Fachinformationszentrum Karlsruhe, 76344 Eggenstein-Leopoldshafen, Germany, (fax: +49 7247 808 666; e-mail: crysdata@fiz.karlsruhe.de) on quoting the depository number CSD-420881 and 420882.

Table 4
Atomic coordinates and isotropic displacement parameters for $Gd_5Ga_{1.0}Ge_{3.0}$ as obtained by single crystal X-ray diffraction at 298 and 533 K.

Atom		x	y	z	U_{eq}, (Å^2)[a]
298 K					
Gd1	8d	0.0136(1)	0.5954(1)	0.1819(1)	0.013(1)
Gd2	8d	0.3285(1)	0.1219(1)	0.1730(1)	0.013(1)
Gd3	4c	0.1633(2)	1/4	0.5109(2)	0.014(1)
T1	8d	0.1664(3)	0.4597(1)	0.4672(2)	0.016(1)
T2	4c	0.0324(4)	1/4	0.1086(3)	0.015(1)
T3	4c	0.2819(4)	1/4	0.8686(3)	0.013(1)
533 K					
Gd1	8d	0.0294(2)	0.5904(1)	0.1649(2)	0.021(1)
Gd2	8d	0.3066(2)	0.1167(1)	0.1833(2)	0.018(1)
Gd3	4c	0.1343(3)	1/4	0.5155(3)	0.018(1)
T1	8d	0.1350(4)	0.4532(2)	0.4878(4)	0.022(1)
T2	4c	0.0078(6)	1/4	0.1082(6)	0.021(1)
T3	4c	0.2529(7)	1/4	0.8784(6)	0.025(1)

[a] U(eq) is defined as one third of the trace of the orthogonalized U_{ij} tensor.

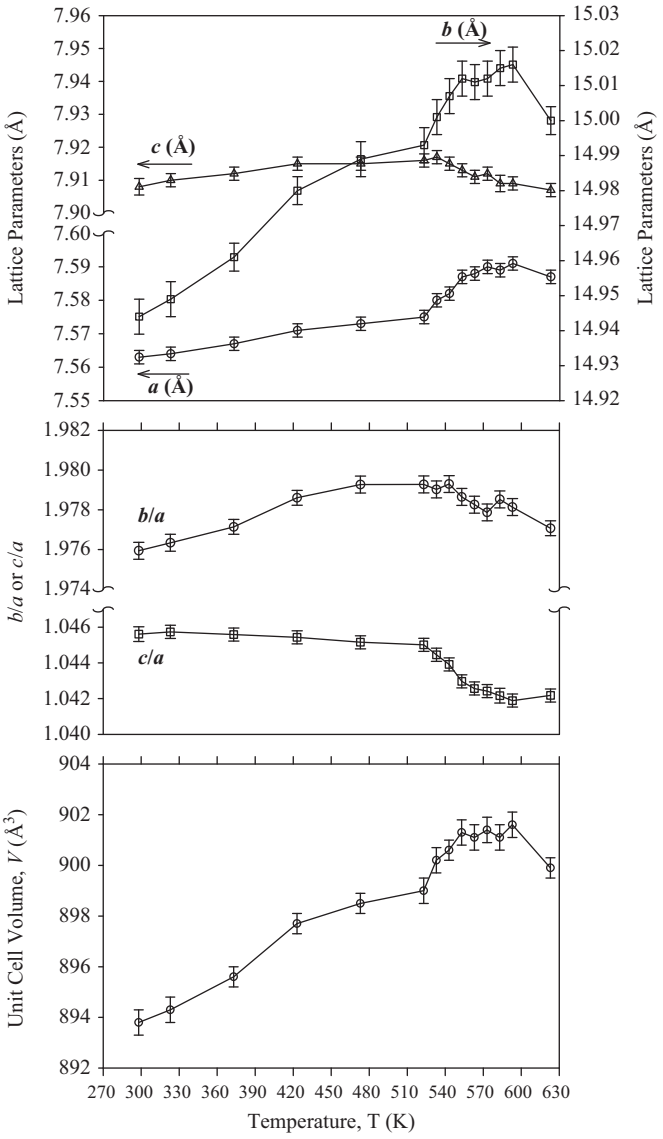

Fig. 6. Lattice parameters of $Gd_5Ga_{1.0}Ge_{3.0}$ as a function of temperature as obtained from powder X-ray diffraction.

3.3. Phase transformations in $Gd_5Ga_{1.0}Ge_{3.0}$

Lattice parameters and atomic coordinates for $Gd_5Ga_{1.0}Ge_{3.0}$ at 298 and 533 K from single crystal X-ray diffraction experiments are listed in Tables 3 and 4. Fig. 6 shows the lattice parameters for $Gd_5Ga_{1.0}Ge_{3.0}$ obtained from powder X-ray diffraction for the temperature range 298–623 K. Room temperature crystal structure of $Gd_5Ga_{1.0}Ge_{3.0}$ belongs to the Pu_5Rh_4-type, which is made up of [Gd_5T_4] (T = Ge and/or Ga) slabs, similar to those found in any of the established crystal structures of the $Gd_5(Si_xGe_{1-x})_4$ series. The interslab dimer distances for the Pu_5Rh_4-type structure lie between the Gd_5Si_4- and Sm_5Ge_4-type structures. From previous investigations [21], we have observed

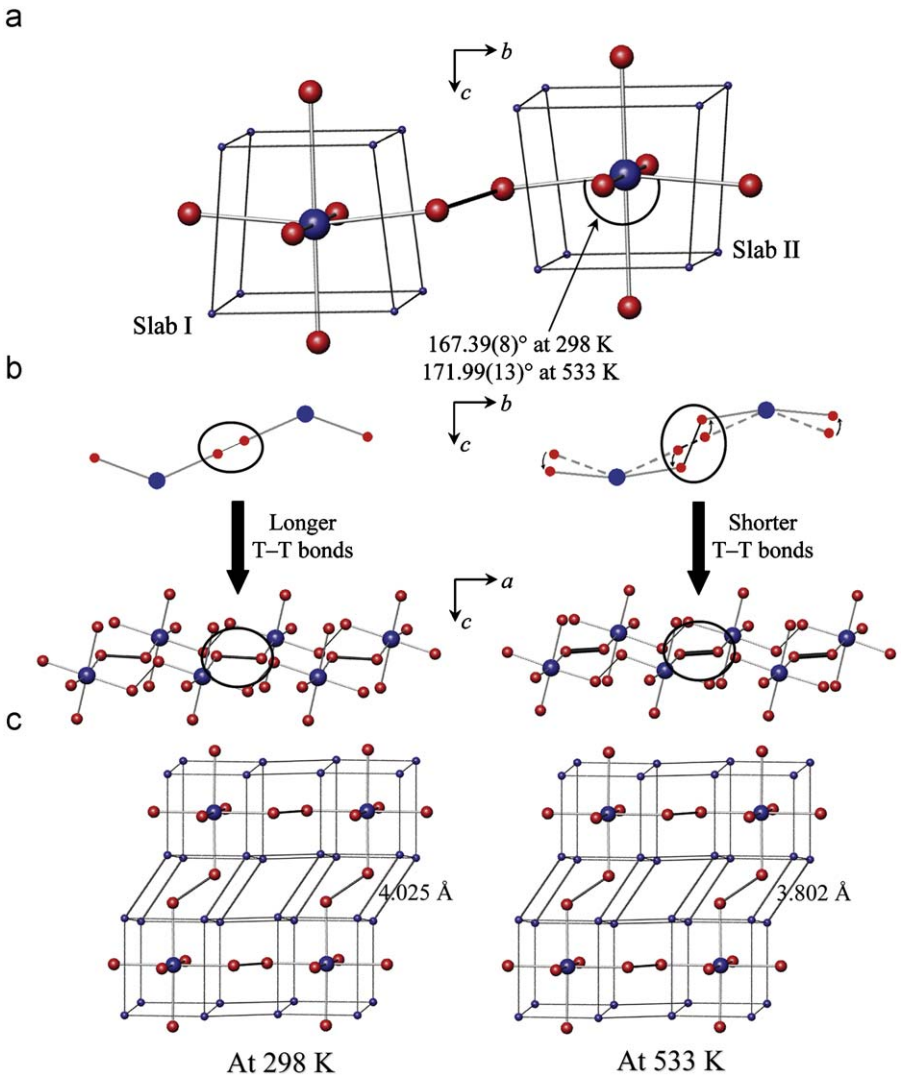

Fig. 7. (a) Change in T1–Gd3–T1 bond angle for $Gd_5Ga_{1.0}Ge_{3.0}$ as the temperature varies from 298 to 533 K. (b) Schematic diagram in two different orientations depicting how the change in bond angle decreases the T1–T1 distance. (c) Variation of interslab contacts with temperature for $Gd_5Ga_{1.0}Ge_{3.0}$.

that this particular phase is placed at the top end of the discontinuous part of the c/a vs. x plot (Fig. 1). Combined with this, the results of low-temperature X-ray diffraction of $Gd_5Ga_{0.7}Ge_{3.3}$ directed us to expect that upon heating $Gd_5Ga_{1.0}Ge_{3.0}$, the interslab T1–T1 bond distances would increase and possibly cleave, leading to a Sm_5Ge_4-type structure.

In fact, a first look at the variations of b/a, c/a, and V (Fig. 6) with temperature based on high-temperature powder X-ray diffraction experiments indicate a similar sort of phase transformation as the lattice parameter ratios decrease and the unit cell volume increases abruptly for $T > 523$ K. This outcome could be attributed simply to an increase in the a lattice parameter and, hence, an increase in the T1–T1 dimer distance. A closer look at the data from both powder and single crystal X-ray diffraction; however, shows that an increase in the a parameter is accompanied, as expected, by an increase in the b parameter, but, unlike what has been observed in other RE_5T_4 materials [19], the c parameter decreases. Between 523 and 593 K, the powder X-ray data reveal a 0.21% and 0.15% increase in the a- and b-lengths, respectively. On the other hand, for the same temperature range, there is 0.09% decrease in the c-axis. Combining these three trends produces a 0.29% increase in the unit cell volume. This change can be visualized as applying a pressure to an oriented metal block along the c-direction with no restrictions along the a- and b-direction. This forces the slabs to slide closer to each other along the c-direction. The result is a decrease in the T1–T1 interslab distance, which lies nearly perpendicular to the c-direction, from 2.837(4) to 2.521(7) Å (Table 3).

Apart from this severe change in interslab dimer distance, there are some subtle structural changes which help us better understand this phase transition from the Pu_5Rh_4-type to Gd_5Si_4-type structure. First, consider the fragment, shown in Fig. 7a and based on single crystal X-ray diffraction at 298 and 533 K: the T1–Gd3–T1 fragment from slab-I is oriented in a "V" form, whereas the T1–Gd3–T1 fragment from slab-II is oriented in an "inverted V" form and these two fragments are linked by a T1–T1 bond. As temperature is increased, the c-parameter decreases and the T1–Gd3–T1 bond angle increases by 4.6(1)°, both of which brings these linker T1 atoms of the two fragments closer to each other (Fig. 7b). Also affected are the interslab Gd–Gd contacts as shown in Fig. 7c: at 298 K the longer (4.025 Å) Gd1–Gd2 distances shrink to 3.802 Å at 533 K. This feature is in stark contrast to similar characteristics in the $Gd_5(Si_xGe_{1-x})_4$ series, when the Sm_5Ge_4-type (short Gd1–Gd1 interslab distance) transforms to the Gd_5Si_4-type structure (long Gd1–Gd1 interslab distance). This difference is due to the fact that in the $Gd_5(Ga_xGe_{1-x})_4$ scenario

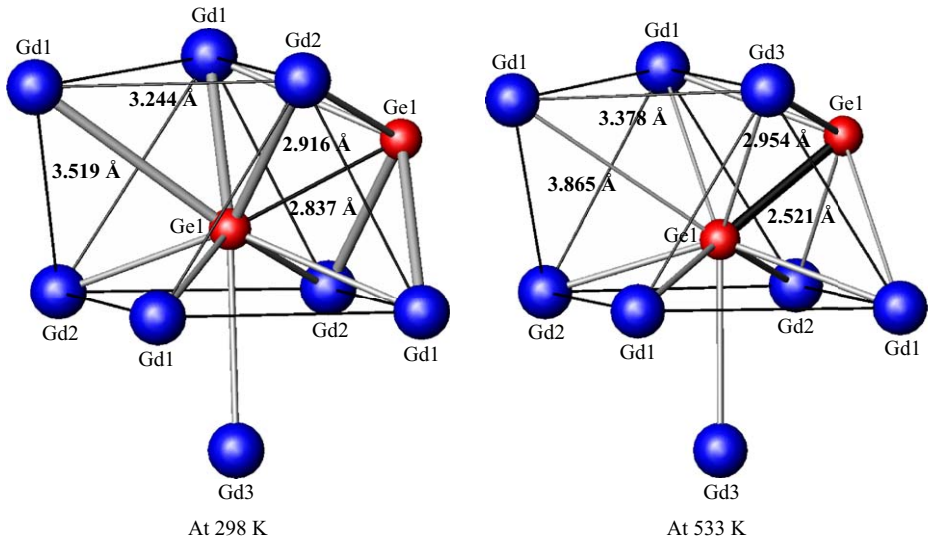

Fig. 8. Coordination environments surrounding the T1 sites for $Gd_5Ga_{1.0}Ge_{3.0}$ as it changes with temperature. Interatomic distances showing significant differences between the structures are included.

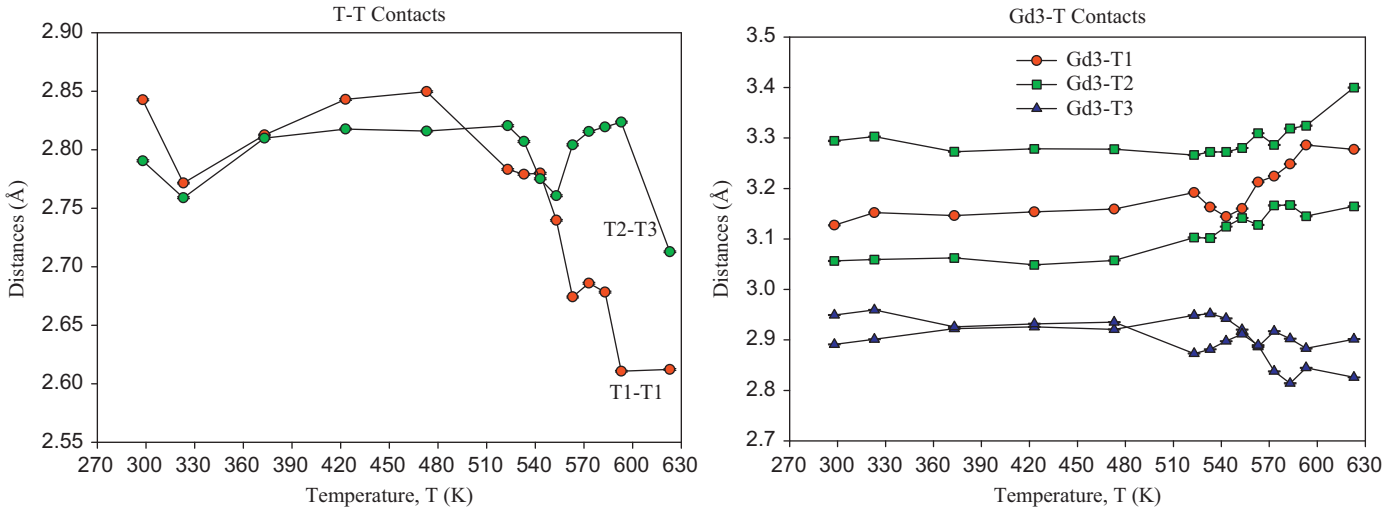

Fig. 9. T–T contact distance variations with temperature in $Gd_5Ga_{1.0}Ge_{3.0}$ as obtained from powder X-ray diffraction experiment.

the *a*- and *c*-parameters change in the opposite direction, which is not the case for the $Gd_5(Si_xGe_{1-x})_4$ series.

The other significant change arises in the coordination environments surrounding the T1 sites as shown in Fig. 8. On heating, the T1–T1 distance decreases for reasons mentioned above, and this promotes the increase of three interslab T1–Gd distances. The T1–Gd1 contact capping the trigonal prism increases from 3.519 to 3.865 Å. The other two, T1–Gd1 and T1–Gd2 contacts within the trigonal prism, also increase to 3.378(4) and 2.954(4) Å, respectively. Thus, Gd–T bonds in the Pu_5Rh_4-type structure are exchanged for T–T and Gd–Gd bonds in the Gd_5Si_4-type structure. Fig. 9 illustrates the trends for some interatomic distances as the material is heated from 298 to 623 K. Related plots for other interatomic distances as the temperature increases are compiled in supporting information. For all plots the distances change abruptly above 523 K, which is the temperature at which the phase transition begins. Although the most notable changes occur for T1–T1 and T2–T3 distances, there are significant changes associated with Gd–T contacts, especially the Gd3–T contacts.

From our single crystal X-ray diffraction experiments, we observe that the crystal (inside the capillary) starts to decompose above 573 K; on cooling, the original structure is not recovered. During corresponding high-temperature powder X-ray diffraction experiments (see Fig. 6); there exists a possibility for partial sample decomposition or reaction with adventitious oxygen, although the atmosphere inside the sample chamber for the powder diffractometer is much better controlled, with respect to the levels of oxygen, nitrogen, and moisture, than the atmosphere inside the capillary. Adventitious oxygen atoms can enter voids located between slabs stacked along the *b*-axis, which could account for the significant decrease in the *b* parameter, as well as drops in *a*, *c*, and volume above 593 K; see also Ref. [34] for similar behavior in $Gd_5Si_2Ge_2$ at high temperatures.

To check the possible structural implications at low temperatures, we also performed single crystal X-ray diffraction on $Gd_5Ga_{1.0}Ge_{3.0}$ (see supporting information) from 298 to 120 K. These experiments do not show any structural transitions down to 120 K.

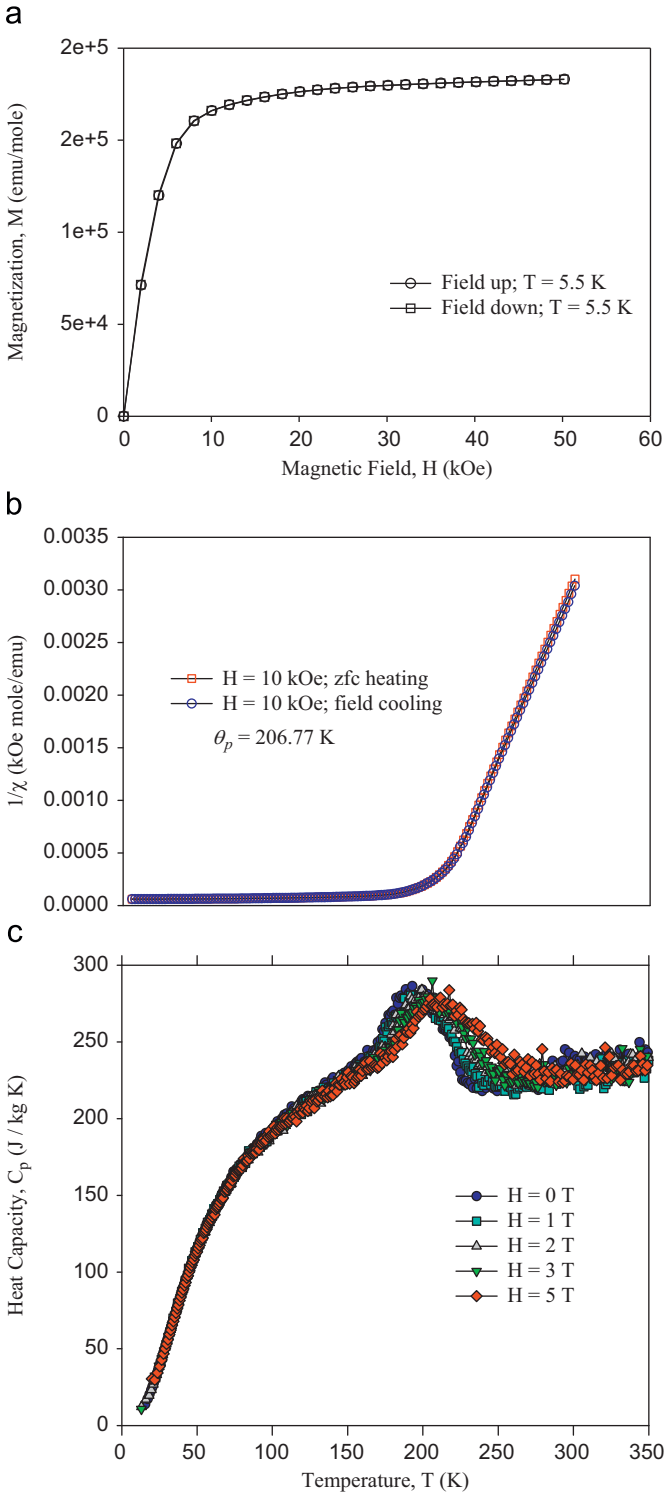

Fig. 10. (a) Isothermal magnetization plot with varying dc magnetic fields measured on a polycrystalline sample of $Gd_5Ga_{1.0}Ge_{3.0}$. (b) Dc inverse magnetic susceptibility vs. temperature plot. (c) The heat capacity of a polycrystalline sample of $Gd_5Ga_{1.0}Ge_{3.0}$ measured in 0, 1, 2, 3, and 5 T magnetic fields after zero-field cooling the sample to ca. 5 K.

3.4. Magnetism and heat capacity for $Gd_5Ga_{1.0}Ge_{3.0}$

Fig. 10a shows the isothermal magnetization plot at a temperature of 5.5 K for varying dc magnetic fields in the range 0–50 kOe. The temperature dependence of the inverse magnetic susceptibility corrected for the diamagnetic and temperature independent paramagnetic susceptibility contribution is shown in Fig. 10b. The paramagnetic Curie temperature, $\theta_p = 206.8(2)$ K, was calculated from the Curie–Weiss behavior of $1/\chi(T)$ dependency observed between ca. 250 and 300 K, above the magnetic ordering temperature.

The temperature variation of the heat capacity (C_p) of a polycrystalline sample of $Gd_5Ga_{1.0}Ge_{3.0}$ is also shown in Fig. 10c. The $C_p(T)$ data show a non λ-type anomaly peaking at ca. 190 K similar to $Gd_5Ga_{0.7}Ge_{3.3}$. With increasing magnetic field, the position of the $C_p(T)$ peak shifts towards higher temperatures, a behavior which corroborates the ferromagnetic nature of the magnetic ordering. Its broad feature may be due to the inhomogeneity of as-cast samples which were used for these measurements.

4. Conclusions

In situ low-temperature diffraction experiments on $Gd_5Ga_{0.7}Ge_{3.3}$ show a structural phase transition from Sm_5Ge_4-type to $Gd_5Si_2Ge_2$-type and then to Gd_5Si_4-type as temperature decreases. On the other hand, *in situ* high-temperature diffraction experiments on $Gd_5Ga_{1.0}Ge_{3.0}$ show a structural phase transition from Pu_5Rh_4-type to Gd_5Si_4-type as temperature rises. These temperature-induced structural transformations in the $Gd_5Ga_xGe_{4-x}$ system reveal the immense flexibility of this system. These results also present, for the first time, the existence of orthorhombic Sm_5Ge_4-, monoclinic $Gd_5Si_2Ge_2$- and Gd_5Si_4-type, for the same composition.

Acknowledgments

The authors thank Prof. Vitalij Pecharsky, Dr. Yaroslav Mudryk, Dr. Niraj Singh, and Mr. Roger Rink for making the SQUID Magnetometer, semi-adiabatic heat-pulse calorimeter, and Rigaku TTRAX diffractometer available to us and for informative discussions. This work was carried out at the Ames Laboratory, which is operated for the US Department of Energy by Iowa State University under Contract no. DE-AC02-07CH11358. This work was supported by the Materials Sciences Division of the Office of Basic Energy Sciences of the US Department of Energy.

Appendix A. Supplementary material

Supplementary data associated with this article can be found in the online version at doi:10.1016/j.jssc.2009.08.016.

References

[1] V.K. Pecharsky, K.A. Gschneidner Jr., Phys. Rev. B 78 (1997) 4494.
[2] V.K. Pecharsky, K.A. Gschneidner Jr., Appl. Phys. Lett. 70 (1997) 3299.
[3] V.K. Pecharsky, K.A. Gschneidner Jr., J. Magn. Magn. Mater. 167 (1997) L179.
[4] G.J. Miller, Chem. Soc. Rev. 35 (2006) 799.
[5] A. Giguere, M. Foldeaki, R. Ravi Gopal, T.K. Bose, A. Frydman, Phys. Rev. Lett. 83 (1999) 2262.
[6] K.A. Gschneidner Jr., V.K. Pecharsky, H.G.M. Duijin, E.M. Levin., Phys. Rev. Lett. 85 (2000) 4190.
[7] A.O. Pecharsky, K.A. Gschneidner Jr., V.K. Pecharsky, J. Appl. Phys. 93 (2003) 4722.
[8] K.A. Gschneidner Jr., V.K. Pecharsky, A.O. Tsokol, Rep. Prog. Phys. 68 (2005) 1479.
[9] L. Morellon, J. Blasco, P.A. Algarabel, M.R. Ibara, Phys. Rev. B 62 (2000) 1022.
[10] L. Morellon, P.A. Algarabel, M.R. Ibara, J. Blasco, B. Garcia-Landa, Phys. Rev. B 58 (1998) R14721.
[11] C. Magen, L. Morellon, P.A. Algarabel, C. Marquina, M.R. Ibara, J. Phys. Condens. Matter 15 (2003) 2389.

[12] L. Morellon, J. Stankiewicz, B. Garcia-Landa, P.A. Algarabel, M.R. Ibara, Appl. Phys. Lett. 73 (1998) 3462.
[13] E.M. Levin, V.K. Pecharsky, K.A. Gschneidner Jr., Phys. Rev. B 60 (1999) 7993.
[14] E.M. Levin, V.K. Pecharsky, K.A. Gschneidner Jr., J. Magn. Magn. Mater. 210 (2000) 181.
[15] E.M. Levin, V.K. Pecharsky, K.A. Gschneidner Jr., Phys. Rev. B 63 (2001) 174110.
[16] J. Stankiewicz, L. Morellon, P.A. Algarabel, M.R. Ibara, Phys. Rev. B 61 (2000) 12651.
[17] W. Choe, V.K. Pecharsky, A.O. Pecharsky, K.A. Gschneidner Jr., V.G. Young Jr., G.J. Miller, Phys. Rev. Lett. 84 (2000) 4617.
[18] J. Meyer, S. Chumbley, W. Choe, G.J. Miller, Phys. Rev. B 66 (2002) 012106/012101.
[19] W. Choe, A.O. Pecharsky, M. Wörle, G.J. Miller, Inorg. Chem. 42 (2003) 8223.
[20] S. Misra, G.J. Miller, J. Solid State Chem. 179 (2006) 2290.
[21] Y. Mozharivskyj, W. Choe, A.O. Pecharsky, G.J. Miller, J. Am. Chem. Soc. 125 (2003) 15183.
[22] L.M. Wu, S.H. Kim, D.K. Seo, J. Am. Chem. Soc. 127 (2005) 15682.
[23] W. Choe, G.J. Miller, J. Meyers, S. Chumbley, A.O. Pecharsky, Chem. Mater. 15 (2003) 1413.
[24] G.S. Smith, Q. Johnson, A.G. Tharp, Acta Crystallogr. 22 (1967) 269.
[25] F. Holtzberg, R.J. Gambino, T.R. McGuire, J. Phys. Chem. Solids 28 (1967) 2283.
[26] A.O. Pecharsky, K.A. Gschneidner Jr., V.K. Pecharsky, C.E. Schindler, J. Alloys Compd. 338 (2002) 126.
[27] V. Svitlyk, G.J. Miller, Y. Mozharivskyj, J. Am. Chem. Soc. 131 (2009) 2367.
[28] V.K. Pecharsky, G.D. Samolyuk, V.P. Antropov, A.O. Pecharsky, K.A. Gschneidner Jr., J. Solid State Chem. 171 (2003) 57.
[29] J. Le Roy, J.M. Moreau, D. Paccard, E. Parthe, Acta Crystallogr. B 34 (1978) 3315.
[30] Materials Preparation Center, Ames Laboratory, US DOE Basic Energy Sciences, Ames, IA, USA. see 〈www.mpc.ameslab.gov〉.
[31] T.A. Lograsso, D.L. Schlagel, A.O. Pecharsky, J. Alloys Compd. 393 (2005) 141.
[32] W. Kraus, G. Nolze, Powder cell for windows, version 2.4, 2000.
[33] B.A. Hunter, IUCR Powder Diffr. 22 (1997).
[34] Y. Mozharivskyj, A.O. Pecharsky, V.K. Pecharsky, G.J. Miller, J. Am. Chem. Soc. 127 (2005) 317.
[35] XRD Single Crystal Software; Bruker Analytical X-ray Systems, Madison, USA, 2002.
[36] V.K. Pecharsky, J.O. Moorman, K.A. Gschneidner Jr., Rev. Sci. Instrum. 68 (1997) 4196.
[37] K.W. Richter, H.F. Franzen, J. Solid State Chem. 150 (2000) 347.
[38] S. Misra, G.J. Miller, J. Am. Chem. Soc. 130 (2008) 13900.
[39] S. Misra, E.T. Poweleit, G.J. Miller, Z. Anorg. Allg. Chem. 635 (2009) 889.